The Astrophysical Journal, 772:31 (11pp), 2013 July 20 doi:10.1088/0004-637X/772/1/31

PROPER MOTIONS AND ORIGINS OF AXP 1E 2259+586 AND AXP 4U 0142+61

Shriharsh P. Tendulkar[1], P. Brian Cameron[2], and Shrinivas R. Kulkarni[1]
[1] California Institute of Technology, 1200 E California Blvd, MC 249-17, Pasadena, CA 91125, USA; spt@astro.caltech.edu, srk@astro.caltech.edu
[2] The Aerospace Corporation, 15049 Conference Center Drive, Chantilly, VA 20151-3824, USA; pbc@astro.caltech.edu
Received 2013 February 10; accepted 2013 May 20; published 2013 July 2

ABSTRACT

Using high-resolution NIR images supported by laser guide star adaptive optics from the Keck II telescope from 2005 to 2012, we have measured the proper motions of two anomalous X-ray pulsars, AXP 1E 2259+586 and AXP 4U 0142+61. The proper motion of AXP 1E 2259+586 in the sky frame is $(\mu_\alpha, \mu_\delta) = (-6.4 \pm 0.6, -2.3 \pm 0.6)$ mas yr^{-1} and that of AXP 4U 0142+61 is $(\mu_\alpha, \mu_\delta) = (-4.1 \pm 1, 1.9 \pm 1)$ mas yr^{-1}. After correcting for the velocity of the progenitors, we calculate the tangential ejection velocities of the magnetars to be 157 ± 17 km s^{-1} and 102 ± 26 km s^{-1} respectively. The proper motion vector of AXP 1E 2259+586 is directed away from the putative center of the supernova remnant CTB 109 that has long been proposed to be associated with AXP 1E 2259+586. This is significant evidence for linking the pulsar with CTB 109. We comment on the possible movement of CTB 109 after the explosion. We narrow the search cone for the birthsite or remnant of AXP 4U 0142+61 to an opening angle of 24°. However, we are unable to find any suitable association.

Key words: instrumentation: adaptive optics – ISM: individual objects (CTB 109) – stars: individual (AXP 1E 2259+586, AXP 4U 0142+61) – stars: magnetars – techniques: high angular resolution

Online-only material: color figures

1. INTRODUCTION

Magnetars were proposed (Thompson & Duncan 1995, 1996) to explain the phenomena of soft gamma repeaters (SGRs) and anomalous X-ray pulsars (AXPs). Unlike canonical pulsars powered by their rotational energy, the dominant energy reservoir of magnetars was their magnetic field density (with magnetic field strength, $B \sim 10^{14}$ G). The magnetar model explained the short soft γ-ray bursts of SGRs to be from violent magnetic reconnection events and the anomalously high X-ray luminosity of AXPs was attributed to the heating of the crust due to the decaying magnetic field. For recent reviews of observational and theoretical progress in the field we refer the readers to Mereghetti (2008) and Rea & Esposito (2011).

The magnetar model is a consistent explanation of many phenomena associated with SGRs and AXPs. However, the processes leading to the formation of a magnetar (as compared to a canonical neutron star) are not well understood. The diversity in progenitor masses (Ritchie et al. 2010; Davies et al. 2009; Bibby et al. 2008; Muno et al. 2006) and the lack of evidence for hyper-energetic supernova (Vink & Kuiper 2006) suggest that other factors such as stellar spin and binarity may be involved.

The large offsets between early SGRs and their putative supernova remnants (SNRs) and the idea that some halo SGRs could explain a fraction of the soft gamma-ray bursts (GRBs) led to the expectation that magnetars have large space velocities of ∼1000 km s^{-1} (see Rothschild & Lingenfelter 1996). This expectation was consistent with the hyper-energetic supernovae and fast rotation predicted by the magnetar model (Thompson & Duncan 1995, 1996). It was proposed that asymmetric neutrino emission from the supernova could provide the required kick (Bisnovatyi-Kogan 1996). This would imply that the kinematics of magnetars are very different from those of ordinary pulsars with space velocities between 250 and 300 km s^{-1} (Hansen & Phinney 1997).

We started a program to measure the proper motions of magnetars in the NIR in order to conclusively identify birthsites of magnetars without relying on coincidence arguments and to measure kinematic ages of magnetars and contrast them to the characteristic ages derived from the spin-period evolution. We reported the proper motions of two magnetars: SGR 1806−20 and SGR 1900+14 in Tendulkar et al. (2012, hereafter TCK12). This is the second paper in the series and applies the precision astrometry techniques developed in TCK12 for two AXPs: AXP 1E 2259+586 and AXP 4U 0142+61. Despite the sparseness of these fields as compared to the fields of SGR 1900+14 and SGR 1806−20, we are able to maintain the same level of precision in our measurements with a larger temporal baseline.

The paper is organized as follows. In Section 2, we summarize our knowledge of these two magnetars. In Section 3, we describe our observations, data reduction methodology and analysis techniques for point-spread function (PSF) fitting, relative astrometry and photometry. We present the results in Section 4 and in Section 5 we discuss the significance of our proper motion measurements.

2. TARGETS

Table 1 summarizes the basic details about AXP 1E 2259+586 and AXP 4U 0142+61. In the next two subsections, we summarize our state of knowledge of these two magnetars.

2.1. AXP 1E 2259+586

AXP 1E 2259+586 was discovered by Gregory & Fahlman (1980) as a bright point source (then designated GF 2259+586) at the center of curvature of a 36′ diameter semi-circular arc (then designated G109.1−1.0, now CTB 109). Fahlman & Gregory (1981) reported that the central source was an X-ray pulsar with a period of 3.4890 ± 0.0002 s. Later observations showed that the fundamental period of the pulsar was 6.978725 s (Morini et al. 1988) and it had a spin-down rate of 6.2×10^{-13} s s^{-1} (Koyama et al. 1989).

2.1.1. Optical/IR Counterpart

Hulleman et al. (2001) detected a faint IR source ($K_s = 21.7$) at the refined position from the *Chandra X-ray Observatory*.

Table 1
Characteristics of AXP 1E 2259+586 and AXP 4U 0142+61

	AXP 1E 2259+586	AXP 4U 0142+61
Period P (s)	6.9789484460(39)	8.68832877(2)
$\dot{P}$ (10^{-11} s s^{-1})	0.048430(8)	0.20332(7)
$P/\dot{P}$ (kyr)	460	136
$B_{\rm Surf}$ (10^{14} G)	0.59	1.3
R.A. (J2000)	$23^{\rm h}01^{\rm m}08^{\rm s}.295$	$01^{\rm h}46^{\rm m}22^{\rm s}.407$
Decl. (J2000)	$+58^\circ52'44''.45$	$+61^\circ45'03''.19$

Notes. Refer to http://www.physics.mcgill.ca/~pulsar/magnetar/main.html. Positions are from *Chandra* X-ray observations.

SGR-like X-ray bursts (Kaspi et al. 2002a, 2003) on 2002 June 18 and a resultant NIR brightening confirmed the source (Kaspi et al. 2002b) identified by Hulleman et al. (2001). Figure 1 is a $20'' \times 20''$ K_p band image from our data showing the neighborhood of AXP 1E 2259+586. The stars are labeled as per the labeling scheme of Hulleman et al. (2001) with new detections marked with new labels as described in the figure caption.

2.1.2. Characteristics of CTB 109

The location of AXP 1E 2259+586 within $4'$ of the geometric center of CTB 109 (Fahlman & Gregory 1981) and the very small number of X-ray sources in the neighborhood were significant evidence for the association of AXP 1E 2259+586 with CTB 109 with a false coincidence probability of $\approx 10^{-4}$ (Gaensler et al. 2001). The center of the SNR is located at R.A. (J2000) $= 23^{\rm h}01^{\rm m}39^{\rm s}$, decl. (J2000) $= +58^\circ53'00''$ (Kothes et al. 2006). AXP 1E 2259+586 lies at ΔR.A. $\cos\delta = 3'58''$ due west and $\Delta\delta = 16''$ due south of the center of CTB 109.

2.1.3. Distance

There have been multiple recent estimates of the distance to CTB 109 and AXP 1E 2259+586. Kothes & Foster (2012) gathered all observational limits of the distance (from Kothes et al. 2002; Durant & van Kerkwijk 2006; Tian et al. 2010) and estimated a consensus distance of 3.2 ± 0.2 kpc to CTB 109 placing it inside the Perseus spiral arm of the Milky Way.

2.2. AXP 4U 0142+61

AXP 4U 0142+61 was discovered as a soft spectrum X-ray source in the *UHURU* survey (Giacconi et al. 1972). It remained an unexceptional source till 8.7 s X-ray pulsations were discovered through *ASCA* observations by Israel et al. (1993, 1994), including it in the AXP-binarity debate.

2.2.1. Optical/IR Counterpart

Hulleman et al. (2000a) located an optical counterpart ($R = 24.98$ and $I = 23.84$) coincident with the *Einstein* HRI and *ROSAT* position. The presence of optical pulsations at a period of 8.7 s (Kern & Martin 2002) confirmed the source identified by Hulleman et al. (2000a) as the counterpart of AXP 4U 0142+61. Later observations by Hulleman et al. (2004) showed that the counterpart was much brighter in IR with ($K_s = 19.8$) and showed a variability of 0.5 mag over a period of a year. Figure 2 is a $20'' \times 20''$ K_p band image from our data showing the neighborhood of AXP 4U 0142+61. We used the labeled catalog stars as photometric references to calculate the photometric zeropoints for each epoch.

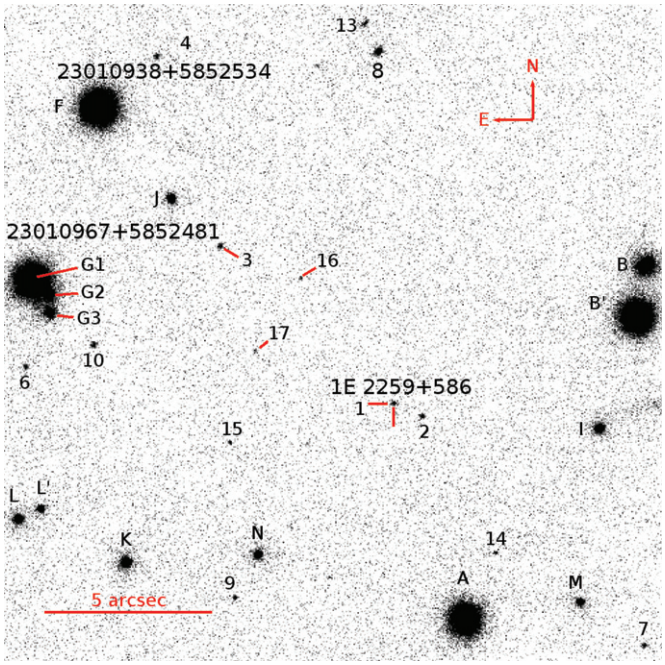

Figure 1. A $20'' \times 20''$ K_p band image around AXP 1E 2259+586 acquired with the NIRC2 camera and the Keck LGS-AO system. Stars are labeled as per Hulleman et al. (2001). Star G of Hulleman et al. (2001) was resolved into three separate stars which we labeled as G1, G2 and G3. Stars 14, 15, 16 and 17 are new to Hulleman et al. (2001) and are labeled afresh. The counterpart to AXP 1E 2259+586 labeled 1 is marked by cross-hairs (colored red in the online version of this paper). The 2MASS stars 2MASS 23010938+5852534 and 2MASS 23010967+5852481 correspond to stars F and the G complex respectively.

(A color version of this figure is available in the online journal.)

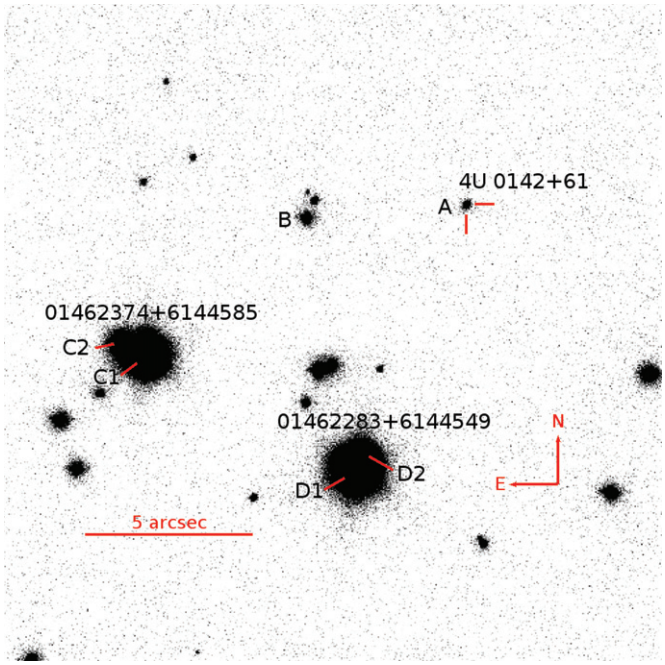

Figure 2. A $20'' \times 20''$ K_p band image around AXP 4U 0142+61 acquired with the NIRC2 camera and the Keck LGS-AO system. Star A is the optical and IR counterpart of AXP 4U 0142+61 as proposed by Hulleman et al. (2000b) and confirmed by Kern & Martin (2002). The 2MASS stars 2MASS 01462374+6144585 and 2MASS 01462283+6144549 are resolved into two components C1, C2 and D1, D2 respectively. The blended magnitudes of the components are used to anchor the zeropoints of the image.

(A color version of this figure is available in the online journal.)

Table 2
Observations of AXP 1E 2259+586

MJD UTC (DDDDD.D YY-MM-DD)	Filt	Airmass	Exp (s)	Notes[a]
53592.428 05-08-10	K_p	1.39	780	A
53592.437 05-08-10	H	1.36	840	F
53639.453 05-09-26	K_p	1.39	1320	A
53919.556 06-07-03	K_p	1.33	1140	A
53920.557 06-07-04	K_p	1.33	1080	F
53964.536 06-08-17	K_p	1.33	1800	AR
54021.299 06-10-13	K_p	1.30	900	A
54089.230 06-12-20	K_p	1.41	1980	A
54262.601 07-06-11	K_p	1.37	960	N
54318.553 07-08-06	K_p	1.31	2100	N
54407.362 07-11-03	K_p	1.42	1260	N
54646.563 08-06-29	K_p	1.34	3060	A
54673.534 08-07-26	K_p	1.29	3000	A
54761.330 08-10-22	K_p	1.30	3600	A
55029.524 09-07-17	K_p	1.32	1800	N
55047.471 09-08-04	K_p	1.33	3600	F
55103.368 09-09-29	K_p	1.29	3420	NG
56070.582 12-05-23	K_p	1.65	1680	NG
56160.463 12-08-21	K_p	1.29	4860	AG
56206.395 12-10-06	K_p	1.32	2340	AG

Notes.
[a] A: Counterpart detected and used for astrometry
F: Counterpart detection was not sufficient for astrometry
G: Glare on the lower right corner of the detector
N: Counterpart not detected
R: Reference image for astrometry and photometry.

Table 3
Observations of AXP 4U 0142+61

MJD UTC (DDDDD.D YY-MM-DD)	Filt	Airmass	Exp (s)	Notes[a]
53639.579 05-09-26	K_p	1.47412	1440.	A
53919.584 06-07-03	K_p	1.70994	2100.	F
53964.593 06-08-17	K_p	1.34345	2100.	AR
54021.550 06-10-13	K_p	1.53298	1500.	A
54089.299 06-12-20	K_p	1.3668	1860.	A
54318.621 07-08-06	K_p	1.34419	660.	A
54407.434 07-11-03	K_p	1.37516	1260.	F
54673.591 08-07-26	K_p	1.4195	1800.	A
54761.444 08-10-22	K_p	1.35228	2400.	A
55029.575 09-07-17	K_p	1.55636	1800.	F
55047.602 09-08-04	K_p	1.36098	2400.	A
55103.454 09-09-29	K_p	1.35571	1920.	FG
56206.446 12-10-06	K_p	1.34739	2700.	AG

Notes.
[a] A: Counterpart detected and used for astrometry
F: Counterpart detection was not sufficient for astrometry
G: Glare on the lower right corner of the detector
N: Counterpart not detected
R: Reference image for astrometry and photometry.

2.2.2. Distance and Neighborhood

Using the red-clump method, Durant & van Kerkwijk (2006) estimated the distance to AXP 4U 0142+61 to be 3.6 ± 0.4 kpc. Radio searches for SNRs in the neighborhood of AXP 4U 0142+61 (Gaensler et al. 2001) failed to detect any emission to a limit of 0.2 mJy beam^{-1} (corresponding to an SNR surface brightness of 3.5×10^{-23} W m^{-2} Hz^{-1} sr^{-1}. AXP 4U 0142+61 is not currently associated with an SNR or a cluster of young stars. With our proper motion measurement, we can narrow down the search to a cone with an opening angle of 24°. We discuss this further in Section 4.

3. OBSERVATIONS AND DATA ANALYSIS

Starting in 2005 to the present time, we undertook a program for astrometric monitoring of magnetars with the 10 m Keck 2 telescope using the laser guide star adaptive optics (LGS-AO; Wizinowich et al. 2006; van Dam et al. 2006) and the Near-Infrared Camera 2 (NIRC2). The log of our observations can be found in Tables 2 and 3.

3.1. NIRC2 Instrument and Observations

The NIRC2 instrument has two modes: wide (W) and narrow (N) with a field-of-view (FoV) of ≈10 × 10 arcsec and ≈40 × 40 arcsec respectively. The corresponding pixel scales are 9.942 mas pixel^{-1} and 39.768 mas pixel^{-1}. In contrast to TCK12, where we used narrow camera images for astrometry, we are constrained to use the wide camera for the astrometry of AXP 1E 2259+586 and AXP 4U 0142+61. The choice of the wide camera was dictated by the low stellar density: there would have been insufficient reference stars in the narrow camera images to perform accurate relative astrometry. The rest of the data analysis procedure is same as TCK12 and is summarized below for completeness.

Based on weather and faintness of each magnetar, multiple short (15 s × 4 coadds) exposures were chosen to avoid saturating the detector. The typical full width at half-maximum (FWHM) achieved in these observations was ≈70 mas ≈2.5 pixel.

Each of the NIRC2 narrow camera images was inspected for quality control. Images in which the AO correction was poor were rejected. The shallow images with acceptable AO correction were rejected for astrometry due to the non-detection of the magnetar and/or lack of sufficient reference stars but were used to photometrically calculate upper limits on the brightness. The images used in the final proper motion measurement are noted by an "A" in Column 5 of Tables 2 and 3.

In observations acquired after 2009 August, a faint glare was observed on the lower right corner (south-west corner) of the detector. The shape and amplitude of the glare was variable with telescope orientation and was not correctable through surface fitting or modeling. The glare was masked in our reduction, thereby improving the astrometry of unmasked stars at the expense of losing a fraction of the stars available for astrometry. The images affected by the glare are flagged with a "G" in Column 5 of Tables 2 and 3.

3.2. Data Analysis

The images from the NIRC2 camera were reduced using the FITS analysis package `pyraf` in a standard manner by subtracting corresponding dark frames and flat-fielded using appropriate dome-flats. A sky fringe frame was made by combining dithered images of multiple targets with the bright stars masked. We used `SExtractor` (Bertin & Arnouts 1996) for the preliminary detection and masking of stars. The fringe frame was subtracted from the flat-fielded data after being scaled to the appropriate sky background level. Before coadding the frames, each frame was corrected for optical distortion using a distortion solution measured for NIRC2.[3]

[3] See http://www2.keck.hawaii.edu/inst/nirc2/forReDoc/post_observing/dewarp/

Table 4
Proper Motions Calculated from the Galactic Rotation Model as Described in Section 3.2.3

Object ID	Distance (kpc)	(l, b) (deg)	$\boldsymbol{\mu}_{\rm Field}$ $[\mu_\alpha, \mu_\delta]$ (mas yr^{-1})	$\boldsymbol{\mu}_{\rm Gal}$ $[\mu_\alpha, \mu_\delta]$ (mas yr^{-1})
AXP 1E 2259+586	3.2 ± 0.2	(109.1, −0.996)	[2.1, 0.63]	$[3.52 \pm 0.1, 0.69 \pm 0.03]$
AXP 4U 0142+61	3.6 ± 0.4	(129.4, −0.431)	[0.97, −0.48]	$[1.48 \pm 0.01, -0.98 \pm 0.06]$

3.2.1. Photometry

Photometry was performed using the `pyraf apphot` toolset as the uncrowded fields did not require the use of PSF fitting. Over the 40″ FoV, the AO PSF varies in shape. To mitigate the effects of the changing PSF on the photometric measurements, we utilized comparison stars within 10″ of the magnetar target over which the PSF is observed not to vary appreciably. The magnitudes of the stars in our images were tied to the measurements from the Two Micron All Sky Survey (2MASS) Point Source Catalog (Skrutskie et al. 2006). In the fields of both AXP 1E 2259+586 and AXP 4U 0142+61, a number of 2MASS stars were found to have companions in our high-resolution images. We calculated a blending correction to the magnitudes measured from the NIRC2 images by combining the magnitudes of each star in a 3″ radius (equal to the FWHM of the 2MASS star images of the magnetar fields). The combined magnitude is calculated as

$$m_{\rm blend} = -2.5 \log_{10} \left(\sum_i 10^{-m_i/2.5} \right),$$

where the m_i is the measured magnitude of the ith star within the blending radius. We used the blended magnitudes to calculate the zeropoints of our images at each epoch and calculate the brightness of the magnetar.

3.2.2. Relative Astrometry

We used the `IDL` package `StarFinder` (Diolaiti et al. 2000) to perform PSF estimation, fitting and subtraction. The images taken on 2006 August 17 were chosen as the reference images on the basis of the good AO performance on that epoch and the faint detection limit. For each epoch, stars detected by `StarFinder` were matched to those from the reference epoch and we concatenated a set of N star positions over E epochs. For AXP 1E 2259+586, $N = 45$, $E = 11$ and for AXP 4U 0142+61, $N = 30$, $E = 9$.

Since NIRC2 is mounted on the Nasmyth focus of the Keck II telescope, a field rotator is used to set the position angle of the field. For each observation, we used a position angle of zero degrees; i.e., north was up and east was to the left on the detector. However, there is a possibility of small changes in the rotator angle. In order to account for these errors, we computed the rotation angle of each stellar grid with respect to the reference grid (from 2006 August 17) and appropriately derotated the grid. The rotation errors were small with a maximum of 0.°2.

As per our astrometric framework described in Cameron et al. (2009) and Tendulkar et al. (2012), we performed simultaneous least-squares fitting of the positions and proper motions of N stars over E epochs. The proper motion of each star is defined with respect to a grid formed by the weighted average position of its neighbors. The matrix of weights is designed to be optimal in the least-squares sense by including the effects of measurement errors and the correlations between star positions expected from the average turbulence profile over Mauna Kea. In TCK12, we have shown that with a reference grid of 50 stars, the systematic error from the choice of the grid is less than 10 μas yr^{-1}.

3.2.3. Galactic Rotation

Since our relative astrometry framework is insensitive to the bulk motion of the field through the sky, we anchored the bulk motion of the field by modeling the rotation of the Milky Way as described in TCK12. The calculated average motion of the field with respect to the sky frame is denoted by $\boldsymbol{\mu}_{\rm Field} = [\mu_\alpha, \mu_\delta]_{\rm Field}$.

In order to trace the movement of the magnetar to its birthsite, we need to know the differential proper motion between the magnetar and its putative progenitor. It is reasonable to assume that the progenitor would likely have been a young massive star and hence would have been moving with the Galactic rotation curve without much dispersion. The maximum velocity dispersion in the velocity dispersion ellipsoid of O and B type main-sequence stars (putative progenitors of magnetars) is 15 km s^{-1} (Dehnen & Binney 1998). We add this velocity dispersion in quadrature with our measurement errors as an additional velocity uncertainty.

We define the peculiar motion of the magnetar as the difference between its total proper motion $\boldsymbol{\mu}_{{\rm Sky},i}$ and its expected Galactic proper motion $\boldsymbol{\mu}_{\rm Gal}$, i.e., $\boldsymbol{\mu}_{{\rm Sky},i} = \boldsymbol{\mu}_{\rm Gal} + \boldsymbol{\mu}_{\rm Pec}$. With this definition, the transverse velocity of the magnetar relative to its neighborhood becomes $r|\boldsymbol{\mu}_{\rm Pec}|$ in a direction θ, s.t. $\tan(\theta) = (\mu_\alpha/\mu_\delta)_{\rm Pec}$ east of north.

Table 4 lists the calculated net proper motion of the field and the proper motion of a putative progenitor at the distance of the magnetar.

4. RESULTS

In this section we present the results of our astrometric and photometric measurements for both magnetars.

4.1. AXP 1E 2259+586

4.2. Astrometry

We performed relative astrometry using a grid of 42 stars over 11 epochs. Of the original 45 stars, it was discovered that the centroiding of three stars located at the edges of the image was corrupted and these stars were velocity outliers. These three stars were removed from the proper motion framework. The robustness of our astrometric framework is demonstrated by the fact that the proper motion measurements changed by $\lesssim$0.1 mas yr^{-1}. Figure 3 shows the measured proper motions of the 42 stars in the field. The field velocity correction, as given in Table 4, was $(\mu_\alpha, \mu_\delta)_{\rm Field} = (2.1, 0.63)$ mas yr^{-1}. The proper motion of the magnetar in the Galactic frame is $(\mu_\alpha, \mu_\delta) = (-6.4 \pm 0.6, -2.3 \pm 0.6)$ mas yr^{-1}. Assuming a distance of 3.2 ± 0.2 kpc, the Galactic proper motion of AXP 1E 2259+586 corresponds to a linear velocity of 103 ± 10 km s^{-1} with an angle of $250^\circ \pm 6^\circ$ east of north. Our measurement is in contrast to the proper motion measurement by Kaplan et al. (2009) from

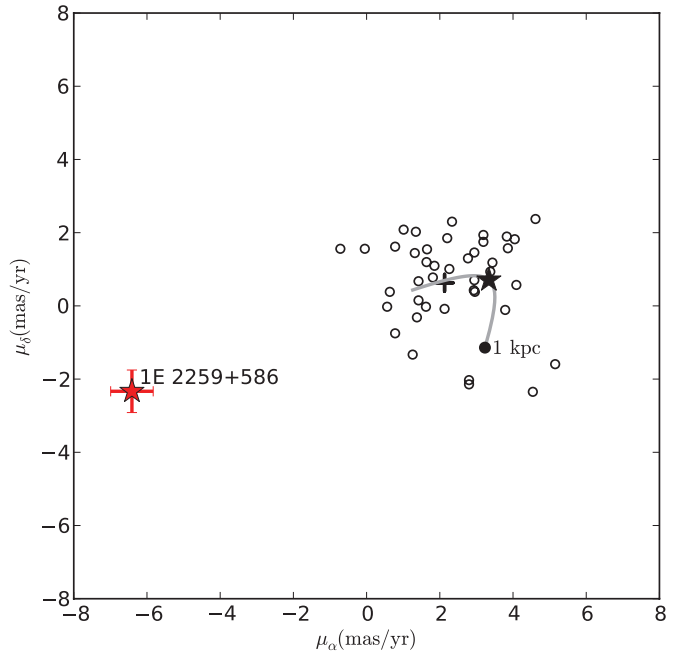

Figure 3. The proper motion of 42 stars in the field of AXP 1E 2259+586 in the sky frame of reference. The counterpart of AXP 1E 2259+586 is marked by the star with error bars (colored red in the online version). The remaining stars have only their best-fit values (hollow black circles) after adding the bulk motion of the field ($\boldsymbol{\mu}_{\rm Field} = (2.1, 0.63)$ mas yr^{-1}) (marked by a black +). The thick gray line represents the expected motion of stars from 1 to 20 kpc along this line of sight, as per the Galactic rotation model presented in Section 3.2.3. The filled black circle at the bottom end of the line denotes the Galactic rotation at 1 kpc away from the Sun. The section of the line representing objects at a distance of 3.2 ± 0.2 kpc from the Sun is marked with a black star and a black line to denote the possible motion of the progenitor of AXP 1E 2259+586.

(A color version of this figure is available in the online journal.)

5 yr baseline *Chandra X-ray Observatory* images. However, we note that their statistical errors (40 mas yr^{-1}) are significantly larger than our precision (0.7 mas yr^{-1}).

The proper motion of AXP 1E 2259+586 away from its birthsite is $(\mu_\alpha, \mu_\delta) = (-9.9 \pm 1.1, -3.0 \pm 1.1)$ mas yr^{-1} including the 15 km s^{-1} dispersion of the putative progenitor. The tangential component of the ejection velocity would be 157 ± 17 km s^{-1}. The proper motion vector is directed away from the center of CTB 109 providing conclusive evidence for the link between AXP 1E 2259+586 and CTB 109.

Figure 4 shows the movement of the magnetar overlaid on an *XMM Newton* mosaic of CTB 109. The current center of the SNR is located at R.A. (J2000) = $23^{\rm h}01^{\rm m}34^{\rm s}$, decl. (J2000) = $+58^\circ53'00''$ (Kothes et al. 2006, quoted without an error estimate). We estimated an error by manually estimating the best fit circle to the outside of the SNR shell. We conservatively estimate that the position of the center is accurate to a radius of $30''$. However, this position cannot be used to estimate a kinematic age for AXP 1E 2259+586 because the apparent centers of SNRs are known to shift due to uneven expansion. We discuss this further in Section 5.

4.3. Photometry

Figure 5 shows the photometric measurements of AXP 1E 2259+586 from 2005 September to 2012 October. AXP 1E 2259+586 has not shown much X-ray or soft γ-ray activity in this period. On 2012 April 28 (MJD 56045), Archibald et al. (2012) detected a factor of two increase in the 1–10 keV flux as compared to the long-term average from *Swift* XRT monitoring and a possibly related event on 2012 April 21 (MJD 56038) from the *Fermi* GBM (Foley et al. 2012). This event is marked in Figure 5 with a vertical line. Despite this activity, we do not see a significant change in the NIR flux of AXP 1E 2259+586. However, the sparse sampling of IR flux and the time separation between the X-ray activity and the IR flux measurement prevent us from drawing significant conclusions about the implications of the difference in IR and X-ray variability.

4.4. AXP 4U 0142+61

4.5. Astrometry

We performed relative astrometry using a grid of 30 stars over 9 epochs. Figure 6 shows the measured proper motions of the 30 stars in the field. The field velocity correction, as given in Table 4, was $(\mu_\alpha, \mu_\delta)_{\rm Field} = (0.97, -0.48)$ mas yr^{-1}. The proper motion of AXP 4U 0142+61 in the Galactic frame is $(\mu_\alpha, \mu_\delta) = (-4.1 \pm 1, 1.9 \pm 1)$ mas yr^{-1}. Assuming a distance of 3.4 ± 0.4 kpc, this corresponds to a tangential velocity of 72 ± 18 km s^{-1}

The proper motion of AXP 4U 0142+61 away from its putative birthsite is $(\mu_\alpha, \mu_\delta) = (-5.6 \pm 1.3, 2.9 \pm 1.3)$ mas yr^{-1}. We calculate the tangential component of the ejection velocity of 102 ± 26 km s^{-1} with an angle of $300^\circ \pm 12^\circ$ east of north.

We attempted to identify a possible birthsite for AXP 4U 0142+61 in the direction opposite to its observed motion. By estimating the age of the magnetar, we can set a limit on the distance that AXP 4U 0142+61 may have moved since its genesis. It is clear that the characteristic age of magnetars calculated from the spin-down rate is not a good metric for the physical age of the pulsars because of the frequent flaring and glitching activity (Woods et al. 2002, 2003). Indeed, in TCK12, we showed that the kinematic age of SGR 1900+14 and SGR 1806−20 was a factor of three to four larger than their characteristic age. The characteristic age of AXP 4U 0142+61 is ∼70 kyr. Hence, it is hard to believe that a potential birthsite/progenitor can be more than about 3×70 kyr $\times$ $6''$ kyr^{-1} $\approx$ $20'$ away from the current location of AXP 4U 0142+61.

From catalogs of OB associations (Mel'Nik & Dambis 2009; Tetzlaff et al. 2010), we identified Cas OB8 as the nearest OB association at a separation of ∼50 arcmin away from AXP 4U 0142+61. The physical size of the cluster is estimated to be 43 pc at an estimated distance of 2 kpc (from catalog by Tetzlaff et al. 2010). The distance of AXP 4U 0142+61 is thus inconsistent with a hypothesis of its genesis in Cas OB8.

Using the SIMBAD database and Aladin, we created a map of all sources around AXP 4U 0142+61 (Figure 7). Table 5 lists all the non-stellar objects in the search cone that have been cataloged. There are two X-ray sources, two radio sources and a few IR sources from *IRAS*. However, each of these sources has only been identified in its respective catalog and there have been no studies of their properties. With the lack of detailed information, we can only estimate the chances of a source being associated with AXP 4U 0142+61 based on its location, motion and an upper limit on the age.

The absence of a detectable SNR or a putative birthsite (possibly an OB association) associated with AXP 4U 0142+61 may result from the old age of AXP 4U 0142+61. From the catalog of Galactic SNRs (Ferrand & Safi-Harb 2012[4]), we note

[4] See http://www.physics.umanitoba.ca/snr/SNRcat/

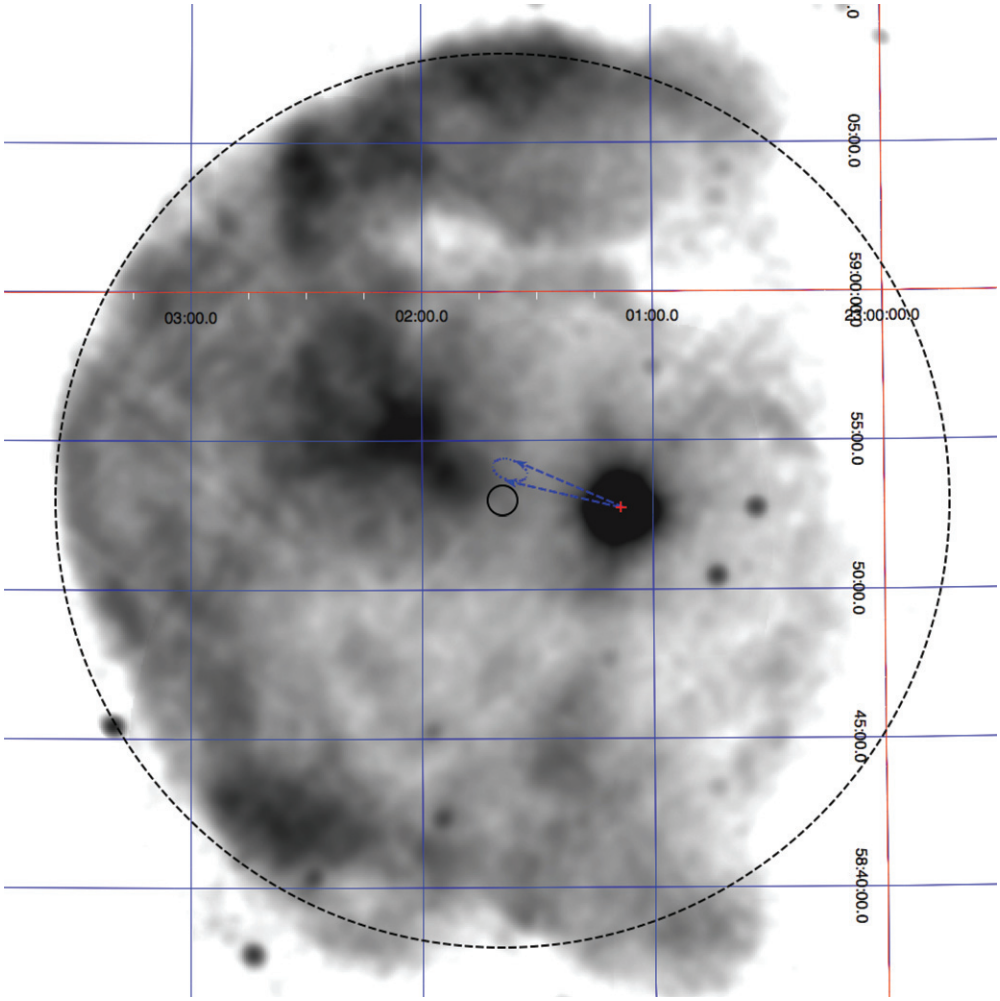

Figure 4. The proper motion of AXP 1E 2259+586 overlaid on an *XMM Newton* image of CTB 109. The dashed black circle denotes the outer extent of the SNR shell. The + symbol (colored red in the online version) marks the position of AXP 1E 2259+586. The solid black circle indicates the center of the SNR with an error radius of 30′. The position of AXP 1E 2259+586 traced backward by 24 ± 5 kyr is indicated by the dashed ellipse (colored blue in the online version).
(A color version of this figure is available in the online journal.)

Table 5
Unidentified and Exotic Objects in the Backward Trace of AXP 4U 0142+61

Object ID	(α, δ) (J2000) (HH:MM:SS DD:MM:SS)	Separation (arcmin)	Kinematic Age (kyr)	Simbad Type
EXMS B0143+613	01:47:00 +61:33:36	12	110	X[a]
1RXS J015020.7+612500	01:50:20.8 +61:25:00	35	330	X
IRAS 01485+6111	01:52:01.4 +61:26:08	45	430	IR
IRAS 01486+6106	01:52:06.8 +61:21:39	47	450	IR
RRF 1305	01:51:45.9 +61:17:04	48	460	Radio
30P 157	01:51:48 +61:17:42	48	460	Radio
IRAS 01493+6114	01:52:49.1 +61:29:41	49	470	IR
IRAS 01505+6112	01:54:06.6 +61:27:43	58	550	IR
IRAS 01502+6101	01:53:44.2 +61:16:17	60	570	IR
IRAS 01498+6055	01:53:21.8 +61:10:35	61	580	IR
Cl Czernik 5	01:55:06 +61:20	67	640	OpCl[b]
IRAS 01514+6058	01:54:57.4 +61:13:19	69	660	IR

Notes.
[a] Not in direct search cone. See Figure 7.
[b] Czernik (1966), diameter = 8′, ∼50 stars.

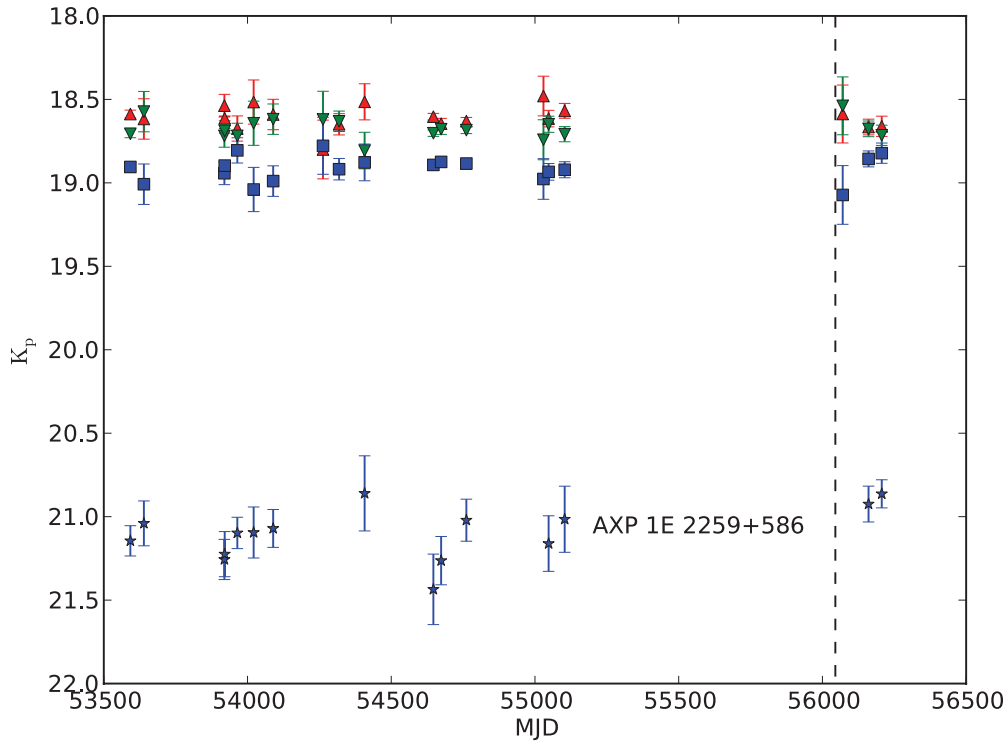

Figure 5. Photometric time series of AXP 1E 2259+586. The stars are identified as per Figure 1. Upright triangles (red in the online version) denote star N, inverted triangles (green in the online version) denote star I and squares (blue in the online version) denote star J. The median brightnesses of these three stars were used to anchor the photometric zeropoints over each epoch. The photometry of the magnetar itself is denoted by blue "*" symbols. The dashed vertical line marks the 2012 April epoch at which X-ray brightening of AXP 1E 2259+586 was observed.

(A color version of this figure is available in the online journal.)

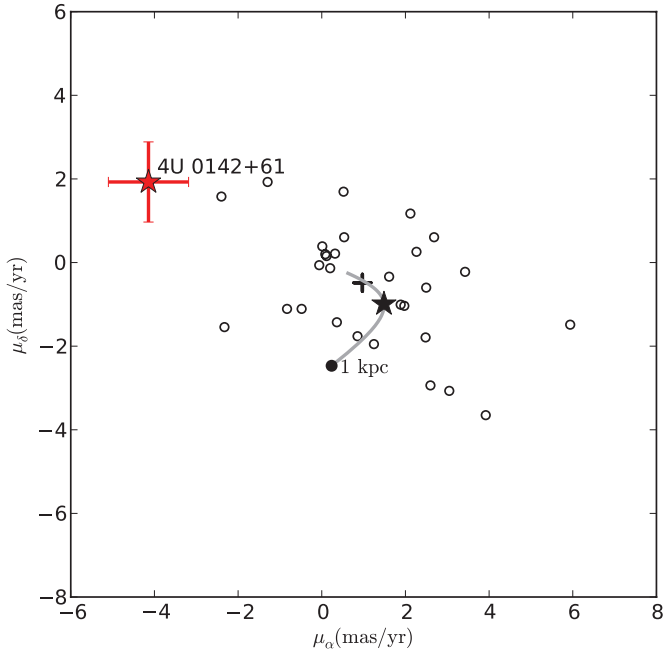

Figure 6. The proper motion of 30 stars in the field of AXP 4U 0142+61 in the sky frame of reference. The counterpart of AXP 4U 0142+61 is marked by the star with error bars (colored red in the online version). The remaining stars have only their best-fit values (hollow black circles) after adding the bulk motion of the field ($\boldsymbol{\mu}_{\rm Field}$ = (0.97, −0.48) mas yr^{-1}) (marked by a black +). The thick gray line represents the expected motion of stars from 1 to 20 kpc along this line of sight, as per the Galactic rotation model presented in Section 3.2.3. The filled black circle at the bottom end of the line denotes the Galactic rotation at 1 kpc away from the Sun. The section of the line representing objects at a distance of 3.2 ± 0.2 kpc from the Sun is marked with a black star and a black line to denote the possible motion of the progenitor of AXP 4U 0142+61.

(A color version of this figure is available in the online journal.)

that only a handful of detectable SNRs, such as Kes 67, W41, G065.1+00.6, G192.8−01.1 and G359.1−00.5, are older than 10^5 yr. It is not unlikely for the SNR shell to diffuse into the interstellar medium (ISM) at such a timescale.

4.6. Photometry

Figure 8 shows the NIR photometry of AXP 4U 0142+61 from 2005 September to 2012 October. Over this period, there have been a series of high-energy activity events associated with AXP 4U 0142+61. Table 6 lists the epochs of the activity. The typical fluences of the burst have been ∼100 counts, which represent very small activity similar to the smallest bursts from AXP 1E 1048−5937 (Kaspi et al. 2006). The quiescent flux of the magnetar did not change significantly through these epochs. The epochs are also plotted in Figure 8 with vertical lines. We measure small (0.5 mag) variations in IR flux through our observations. However, as with AXP 1E 2259+586, we cannot conclusively link them with the X-ray activity due to the sparse sampling and time delays.

5. DISCUSSION

5.1. Proper Motions of the Magnetar Family

Table 7 lists the six available measurements of the tangential space velocities of magnetars. Figure 9 combines the probability distributions (assumed to be Gaussian) of all the six magnetar tangential velocities. The weighted average velocity is 200 km s^{-1} with a weighted standard deviation of 100 km s^{-1}. This is in good agreement with the tangential velocity of the pulsar population which is measured to be 211 km s^{-1} (Hobbs et al. 2005) with a standard deviation of ∼100 km s^{-1}. Thus, the

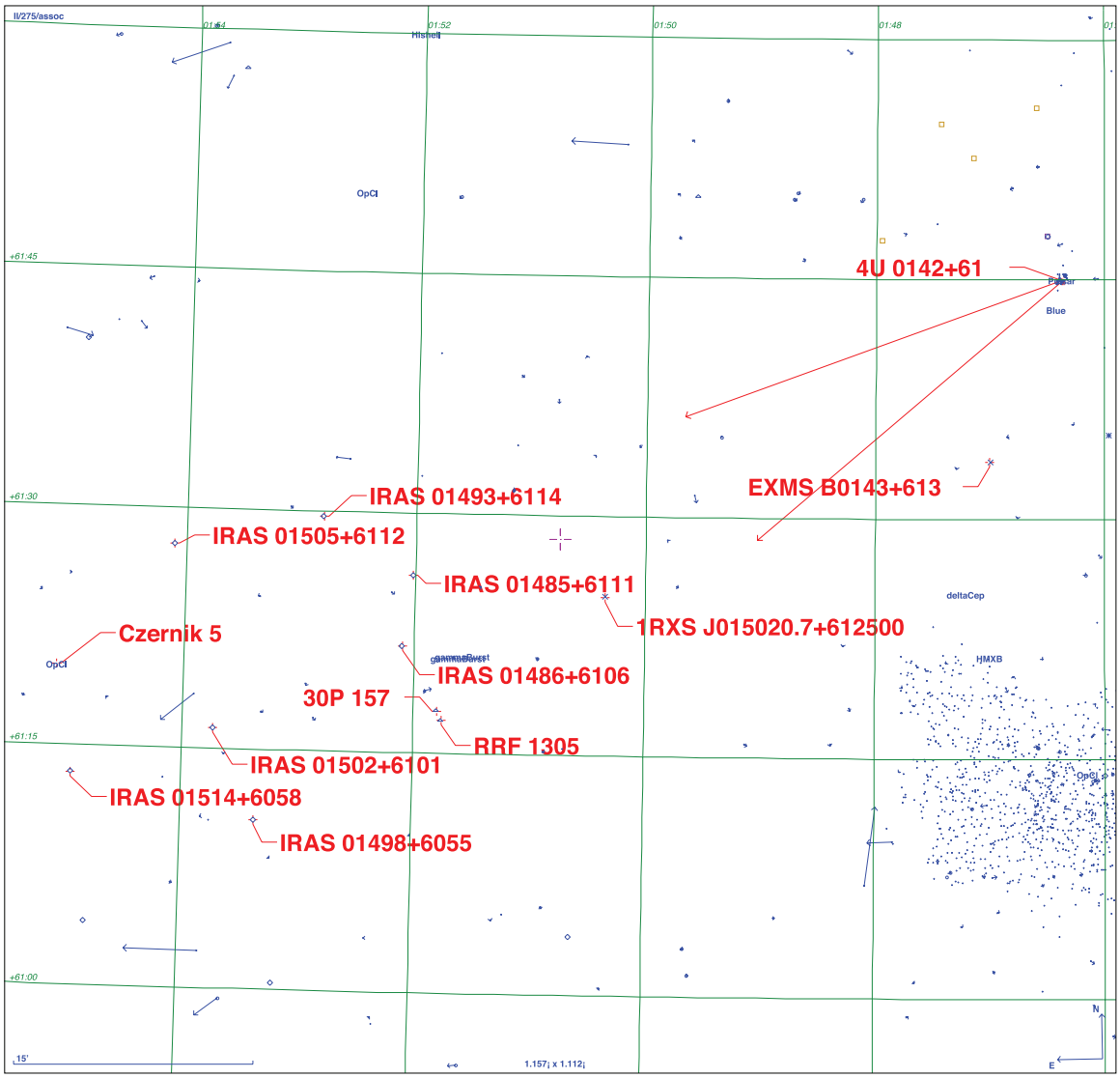

Figure 7. Sources in a $\sim 1^\circ \times 1^\circ$ field to the south-east of AXP 4U 0142+61. The arrows emanating from the position of AXP 4U 0142+61 are the search cone formed by tracing the proper motion of AXP 4U 0142+61 backward in time. Objects identified as stars in the SIMBAD database have not been labeled. We selected all objects that were unidentified from the IRAS catalog, *ROSAT* catalog and other accessible databases. For velocity scale, if AXP 4U 0142+61 were to be associated with 1RXS J015020.7+612500, the kinematic age of AXP 4U 0142+61 would be 330 kyr.

(A color version of this figure is available in the online journal.)

Table 6
High-energy Events of AXP 4U 0142+61 between 2005 September and 2012 October

Date	MJD	Flux/Fluence	Activity	Ref.
2006 Apr 6	53831.3	100 counts	*RXTE*/PCA, small burst	Kaspi et al. (2006)
2006 Jun 25	53911.05	100–200 counts	*RXTE*/PCA, four small bursts	Dib et al. (2006)
2007 Feb 7	54138.42	3600 counts s^{-1}	*RXTE*/PCA, burst	Gavriil et al. (2007)
2011 Jul 29	55771	3500 counts s^{-1}	*Swift*/BAT, burst	Oates et al. (2011)
2012 Jan 12	55938	2000 counts s^{-1}	*Swift*/BAT, burst	Barthelmy et al. (2012)

kinematics of magnetars are completely consistent with those of pulsars.

Given this velocity distribution, it is improbable that SGR 0526−66 has a $\sim 10^3$ km s^{-1} velocity. This adds to the growing body of evidence suggesting that SGR 0526−66 may not be associated with SNR N49 (Gaensler et al. 2001; Klose et al. 2004; Badenes et al. 2009; Park et al. 2012). The original expectation of a large natal kick came from the idea that SGR 0526−66 had rapidly moved to the edge of SNR N49 and the since discredited idea that short hard GRBs are from the galactic halo (Rothschild & Lingenfelter 1996). With these measurements, the probability of finding a magnetar with a large ($\sim$1000 km s^{-1}) space velocity is very low and NS kick mechanisms, as enumerated in Lai (2004), may be applicable in a very small fraction of supernovae. Along with the conclusion from Vink & Kuiper (2006) that supernovae associated with magnetars show no evidence of millisecond proto-neutron stars or higher than typical energetics, the idea of what makes

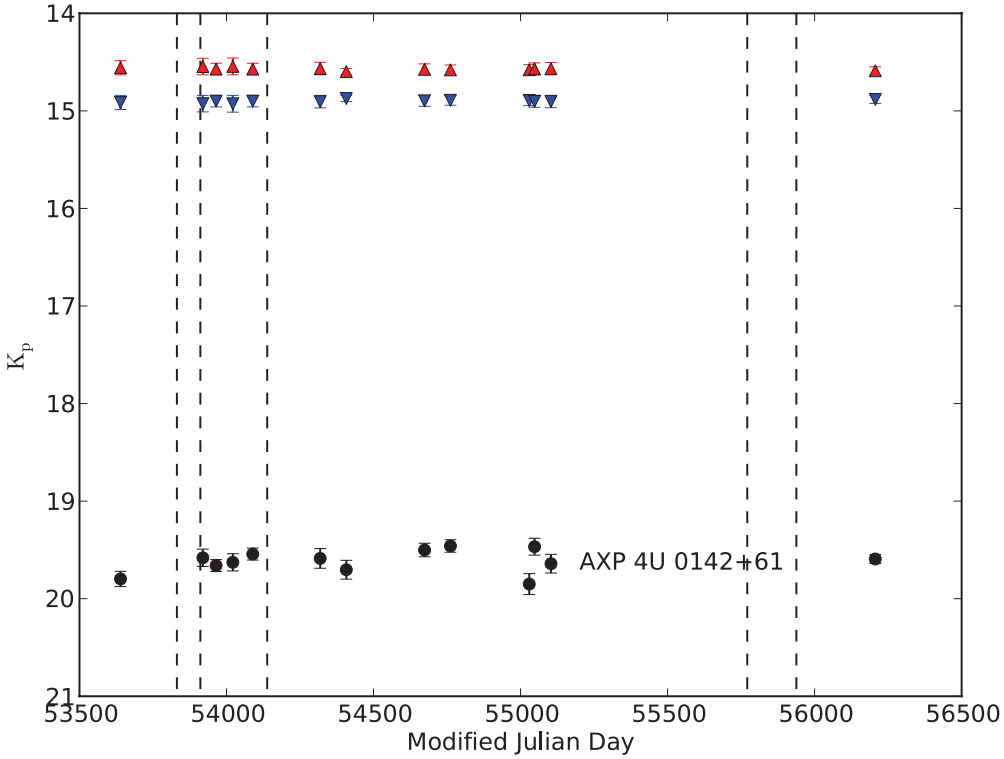

Figure 8. Photometric time series of AXP 4U 0142+61. The K_p magnitude of AXP 4U 0142+61 is denoted by black circles. The photometry was anchored to the brightness of stars C1, C2 and D1, D2 as marked in Figure 2. The photometry is corrected to account for the blending of the stars. The photometry of C1 is denoted by inverted triangles (colored blue in the online version of the paper) and the photometry of D1 is denoted by upright triangles (colored red in the online version). The dashed vertical lines indicate epochs of X-ray or soft γ-ray activity from AXP 4U 0142+61 as detailed in Table 6.

(A color version of this figure is available in the online journal.)

Table 7
List of All Known Magnetar Proper Motions[a]

Object	$V_{\rm tangent}$ (km s^{-1})	Assoc.	Method	Ref.
AXP 1E 1810−197	212 ± 35	···	Radio; VLBI	Helfand et al. (2007)
AXP 1E 1547.0−5408[b]	280 ± 120	SNR G327.24−0.13	Radio; VLBI	Deller et al. (2012)
SGR 1900+14	130 ± 30	Cluster	NIR; LGSAO	Tendulkar et al. (2012)
SGR 1806−20	350 ± 100	Cluster	NIR; LGSAO	Tendulkar et al. (2012)
AXP 1E 2259+586	157 ± 17	SNR CTB 109	NIR; LGSAO	This work
AXP 4U 0142+61	102 ± 26	···	NIR; LGSAO	This work

Notes.
[a] These are the tangential components of the ejection velocities.
[b] Also known as PSR J1550−5418.

magnetar-creating supernovae different from pulsar-creating supernovae need to be revisited.

5.2. Age of CTB 109 and AXP 1E 2259+586

There has been much recent work to estimate the age of CTB 109. Sasaki et al. (2004) modeled the shell of CTB 109 as a Sedov–Taylor shock with data from deep *XMM Newton* observations. They estimate the age of CTB 109 to be 8.8 ± 1 kyr. More recent work by M. Sasaki et al. (2013, in review, private communication) reports the age to be 14 ± 2 kyr. These estimates are in contrast with previous estimates from Wang et al. (1992) (3 kyr; hydrodynamical simulations of X-ray temperature), Rho & Petre (1997) (6–21 kyr; ionization modeling) and Parmar et al. (1998) (3 kyr; ionization modeling and spectra). The consensus put forth by these studies is that the supernova exploded at the eastern edge of a dense giant molecular cloud complex detected in CO by Israel (1980). The western edge of the expanding supernova shell has been slowed and quenched due to its collision with the molecular cloud, and its eastern edge, expanding into a less dense ISM, is significantly less quenched. The apparent center of the expanding shell would be expected to move eastward. We observe this in our measurements.

The separation between the current center of CTB 109 and AXP 1E 2259+586 would correspond to a kinematic age of 24 ± 5 kyr which is significantly larger than the estimated age of CTB 109. This discrepancy implies that the current center of CTB 109 has moved to the east, opposite to the movement of AXP 1E 2259+586. It is more worthwhile to reverse the calculation to find the actual center of the explosion. Assuming the age of the remnant to be 14 ± 2 kyr, we can estimate that AXP 1E 2259+586 moved $2\farcm4 \pm 0\farcm4$ toward the west after the explosion and consequently the current center of CTB 109 would have moved by $1\farcm6 \pm 0\farcm4$ to the east after

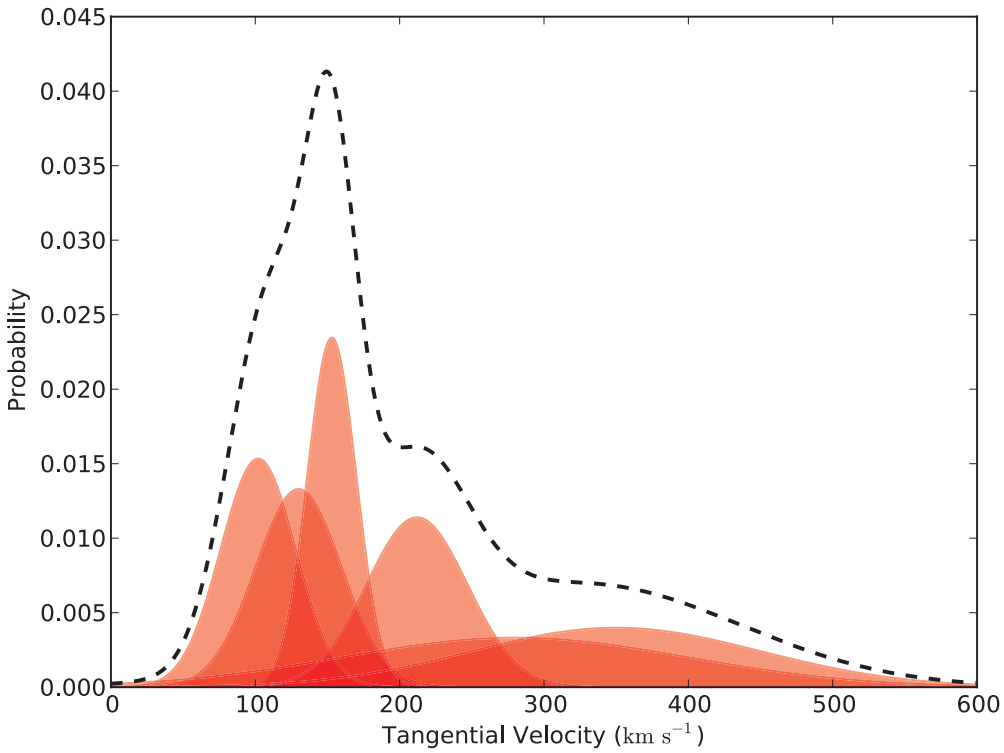

Figure 9. The probability distributions of the tangential velocities of six magnetars as detailed in Table 7 are plotted as filled curves (colored red in the online version). The dashed black line is the sum of the individual probability distributions. The mean and standard deviation of this distribution are 200 km s^{-1} and 100 km s^{-1}. This is very well consistent with the mean and standard deviation of the normal pulsar population (Hobbs et al. 2005).

(A color version of this figure is available in the online journal.)

the explosion. Back calculating from the current position of AXP 1E 2259+586, we estimate that the explosion occurred at $(\alpha, \delta)_{J2000} = (23^h00^m50^s, +58°52'02'')$. The error ellipse at this position has a semi-major axis of $\sigma_{maj} = 26''$, a semi-minor axis of $\sigma_{min} = 15''$ oriented at an angle of 17° south of west.

In conclusion, we have measured the proper motions of two AXPs, AXP 1E 2259+586 and AXP 4U 0142+61, using high resolution NIR images from the LGS-AO supported NIRC2 camera on the Keck II telescope. The tangential components of the ejection velocities of the two magnetars are 157 ± 17 km s^{-1} and 102 ± 26 km s^{-1} respectively. The direction of the proper motion vector of AXP 1E 2259+586 can be traced backward in time to the center of the SNR CTB 109. This is strong evidence that the AXP is associated with the shell. From the estimated age of the SNR and the direction of the magnetar's motion, we estimate that the center of the SNR shell has moved $1.'6 \pm 0.'4$ to the east after the explosion. We narrow the search for the birthsite or remnant associated with AXP 4U 0142+61 to a small cone with a 1σ opening angle of 24°. However, we are unable to locate any object of interest that may be realistically associated with AXP 4U 0142+61. With a sample of six magnetar proper motions, we can calculate the mean and standard deviation of the ejection velocities to be 200 km s^{-1} and 90 km s^{-1} respectively. This corresponds very well with the mean tangential velocities of the general pulsar population of 250 km s^{-1}.

We would like to thank Dr. Manami Sasaki for generously providing the *XMM Newton* mosaic of CTB 109 for Figure 4. The data presented herein were obtained at the W. M. Keck Observatory, which is operated as a scientific partnership among the California Institute of Technology, the University of California and the National Aeronautics and Space Administration. The Observatory was made possible by the generous financial support of the W. M. Keck Foundation.

Facilities: Keck:II(NIRC2), Keck:II(LGS AO)

REFERENCES

Archibald, R. F., Kaspi, V. M., Beardmore, A. P., Gehrels, N., & Kennea, J. 2012, ATel, 4080, 1
Badenes, C., Harris, J., Zaritsky, D., & Prieto, J. L. 2009, ApJ, 700, 727
Barthelmy, S. D., D'Elia, V., Gehrels, N., et al. 2012, GCN, 12829, 1
Bertin, E., & Arnouts, S. 1996, A&AS, 117, 393
Bibby, J. L., Crowther, P. A., Furness, J. P., & Clark, J. S. 2008, MNRAS, 386, L23
Bisnovatyi-Kogan, G. S. 1996, in AIP Conf. Proc. 366, High Velocity Neutron Stars, ed. R. E. Rothschild & R. E. Lingenfelter (Melville, NY: AIP), 38
Cameron, P. B., Britton, M. C., & Kulkarni, S. R. 2009, AJ, 137, 83
Czernik, M. 1966, AcA, 16, 93
Davies, B., Figer, D. F., Kudritzki, R.-P., et al. 2009, ApJ, 707, 844
Dehnen, W., & Binney, J. J. 1998, MNRAS, 298, 387
Deller, A. T., Camilo, F., Reynolds, J. E., & Halpern, J. P. 2012, ApJL, 748, L1
Dib, R., Kaspi, V., Gavriil, F., & Woods, P. 2006, ATel, 845, 1
Diolaiti, E., Bendinelli, O., Bonaccini, D., et al. 2000, Proc. SPIE, 4007, 879
Durant, M., & van Kerkwijk, M. H. 2006, ApJ, 650, 1070
Fahlman, G. G., & Gregory, P. C. 1981, Natur, 293, 202
Ferrand, G., & Safi-Harb, S. 2012, AdSpR, 49, 1313
Foley, S., Kouveliotou, C., Kaneko, Y., & Collazzi, A. 2012, GCN, 13280, 1
Gaensler, B. M., Slane, P. O., Gotthelf, E. V., & Vasisht, G. 2001, ApJ, 559, 963
Gavriil, F. P., Dib, R., Kaspi, V. M., & Woods, P. M. 2007, ATel, 993, 1
Giacconi, R., Murray, S., Gursky, H., et al. 1972, ApJ, 178, 281
Gregory, P. C., & Fahlman, G. G. 1980, Natur, 287, 805
Hansen, B. M. S., & Phinney, E. S. 1997, MNRAS, 291, 569
Helfand, D. J., Chatterjee, S., Brisken, W. F., et al. 2007, ApJ, 662, 1198
Hobbs, G., Lorimer, D. R., Lyne, A. G., & Kramer, M. 2005, MNRAS, 360, 974
Hulleman, F., Tennant, A. F., van Kerkwijk, M. H., et al. 2001, ApJL, 563, L49
Hulleman, F., van Kerkwijk, M. H., & Kulkarni, S. R. 2000a, Natur, 408, 689
Hulleman, F., van Kerkwijk, M. H., & Kulkarni, S. R. 2004, A&A, 416, 1037
Hulleman, F., van Kerkwijk, M. H., Verbunt, F. W. M., & Kulkarni, S. R. 2000b, A&A, 358, 605

Israel, F. P. 1980, AJ, 85, 1612
Israel, G. L., Mereghetti, S., & Stella, L. 1993, IAU Circ., 5889, 1
Israel, G. L., Mereghetti, S., & Stella, L. 1994, ApJL, 433, L25
Kaplan, D. L., Chatterjee, S., Hales, C. A., Gaensler, B. M., & Slane, P. O. 2009, AJ, 137, 354
Kaspi, V., Dib, R., & Gavriil, F. 2006, ATel, 794, 1
Kaspi, V. M., Gavriil, F. P., & Woods, P. M. 2002a, GCN, 1432, 1
Kaspi, V. M., Gavriil, F. P., Woods, P. M., et al. 2003, ApJL, 588, L93
Kaspi, V. M., Jensen, J., Rigaut, F., Hatakeyama, A., & Woods, P. M. 2002b, GCN, 1438, 1
Kern, B., & Martin, C. 2002, Natur, 417, 527
Klose, S., Henden, A. A., Geppert, U., et al. 2004, ApJL, 609, L13
Kothes, R., Fedotov, K., Foster, T. J., & Uyanıker, B. 2006, A&A, 457, 1081
Kothes, R., & Foster, T. 2012, ApJL, 746, L4
Kothes, R., Uyaniker, B., & Yar, A. 2002, ApJ, 576, 169
Koyama, K., Nagase, F., Ogawara, Y., et al. 1989, PASJ, 41, 461
Lai, D. 2004, in Cosmic Explosions in Three Dimensions, ed. P. Höflich, P. Kumar, & J. C. Wheeler (Cambridge: Cambridge Univ. Press), 276
Mel'Nik, A. M., & Dambis, A. K. 2009, MNRAS, 400, 518
Mereghetti, S. 2008, A&ARv, 15, 225
Morini, M., Robba, N. R., Smith, A., & van der Klis, M. 1988, ApJ, 333, 777
Muno, M. P., Clark, J. S., Crowther, P. A., et al. 2006, ApJL, 636, L41
Oates, S. R., Baumgartner, W. H., Beardmore, A. P., et al. 2011, GCN, 12209, 1
Park, S., Hughes, J. P., Slane, P. O., et al. 2012, ApJ, 748, 117
Parmar, A. N., Oosterbroek, T., Favata, F., et al. 1998, A&A, 330, 175
Rea, N., & Esposito, P. 2011, in High-Energy Emission from Pulsars and their Systems, ed. D. F. Torres & N. Rea (Berlin: Springer), 247
Rho, J., & Petre, R. 1997, ApJ, 484, 828
Ritchie, B. W., Clark, J. S., Negueruela, I., & Langer, N. 2010, A&A, 520, A48
Rothschild, R. E., & Lingenfelter, R. E. (ed.) 1996, AIP Conf. Proc. 366, High Velocity Neutron Stars (Melville, NY: AIP)
Sasaki, M., Plucinsky, P. P., Gaetz, T. J., & Bocchino, F. 2013, A&A, 552, A45
Sasaki, M., Plucinsky, P. P., Gaetz, T. J., et al. 2004, ApJ, 617, 322
Skrutskie, M. F., Cutri, R. M., Stiening, R., et al. 2006, AJ, 131, 1163
Tendulkar, S. P., Cameron, P. B., & Kulkarni, S. R. 2012, ApJ, 761, 76
Tetzlaff, N., Neuhäuser, R., Hohle, M. M., & Maciejewski, G. 2010, MNRAS, 402, 2369
Thompson, C., & Duncan, R. C. 1995, MNRAS, 275, 255
Thompson, C., & Duncan, R. C. 1996, ApJ, 473, 322
Tian, W. W., Leahy, D. A., & Li, D. 2010, MNRAS, 404, L1
van Dam, M. A., Bouchez, A. H., Le Mignant, D., et al. 2006, PASP, 118, 310
Vink, J., & Kuiper, L. 2006, MNRAS, 370, L14
Wang, Z., Qu, Q., Luo, D., McCray, R., & Mac Low, M.-M. 1992, ApJ, 388, 127
Wizinowich, P. L., Le Mignant, D., Bouchez, A. H., et al. 2006, PASP, 118, 297
Woods, P. M., Kouveliotou, C., Göğüş, E., et al. 2002, ApJ, 576, 381
Woods, P. M., Kouveliotou, C., Göğüş, E., et al. 2003, ApJ, 596, 464